Supporting Information for

A Universal Principle to Accurately Synthesize Atomically Dispersed Metal-N_4 Sites for CO_2 Electroreduction

Wanzhen Zheng[1, 3], Feng Chen[2], Qi Zeng[1], Zhongjian Li[1], Bin Yang[1, 4], Lecheng Lei[1, 4], Qinghua Zhang[6], Feng He[3], Xilin Wu[2, *], Yang Hou[1, 4, 5, *]

[1]Key Laboratory of Biomass Chemical Engineering of Ministry of Education, College of Chemical and Biological Engineering, Zhejiang University, Hangzhou 310027, People's Republic of China

[2]College of Geography and Environmental Science, Zhejiang Normal University, Jinhua 321004, People's Republic of China

[3]College of Environment, Zhejiang University of Technology, Hangzhou 310014, China

[4]Institute of Zhejiang University - Quzhou, Quzhou 324000, People's Republic of China

[5]Ningbo Research Institute, Zhejiang University, Ningbo 315100, People's Republic of China

[6]Zhejiang Provincial Key Laboratory of Advanced Chemical Engineering Manufacture Technology, College of Chemical and Biological Engineering, Zhejiang University, Hangzhou 310027, People's Republic of China

*Corresponding authors. E-mail: yhou@zju.edu.cn (Yang Hou); dbwxl@zjnu.cn (Xilin Wu)

Supplementary Figures

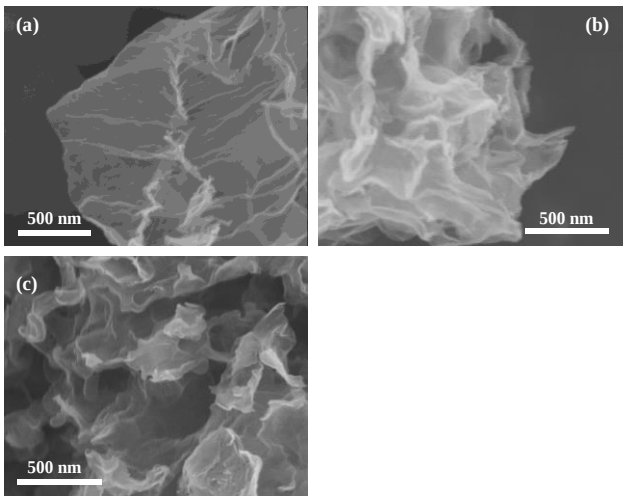

Fig. S1 FESEM images of (**a**) SAs-Fe-N-C, (**b**) SAs-Co-N-C, (**c**) SAs-Cu-N-C

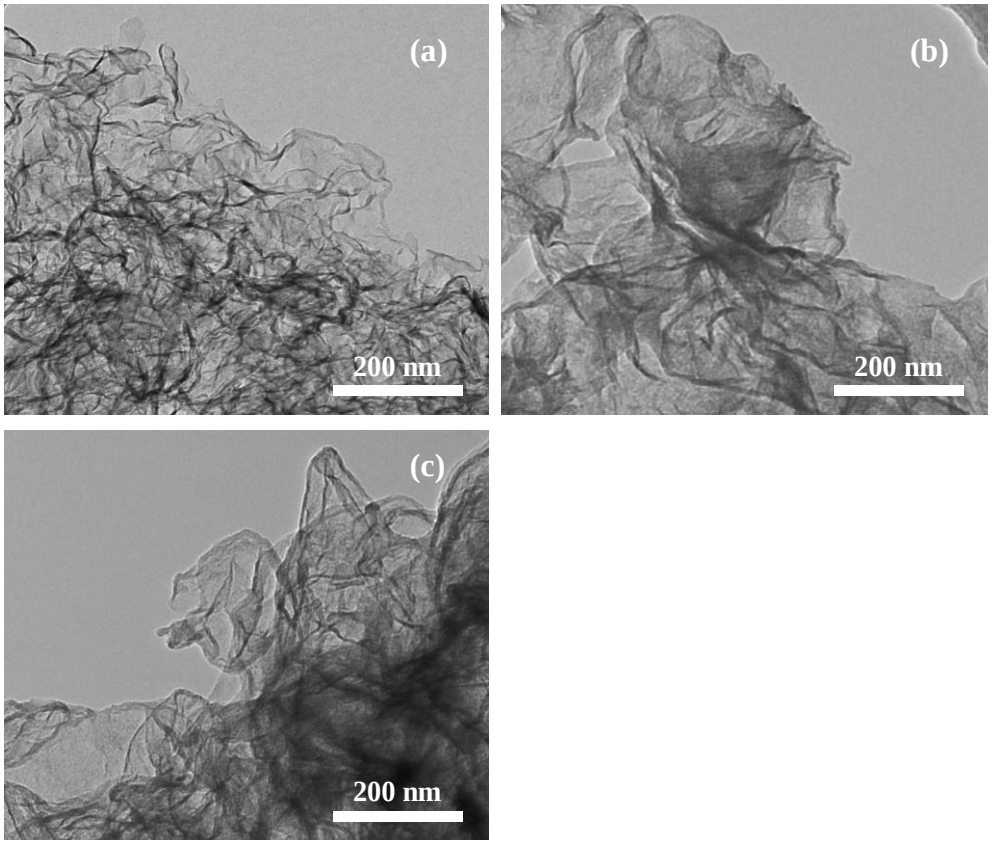

Fig. S2 TEM images of (**a**) SAs-Fe-N-C, (**b**) SAs-Co-N-C, (**c**) SAs-Cu-N-C

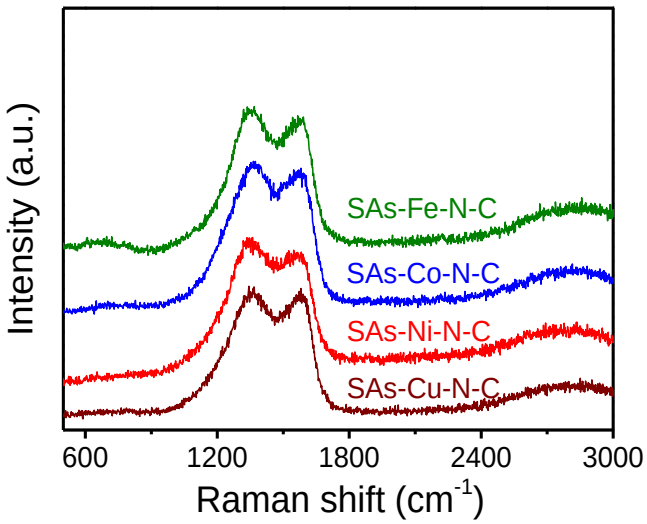

Fig. S3 Raman spectra of SAs-Fe-N-C, SAs-Ni-N-C, SAs-Co-N-C, and SAs-Cu-N-C

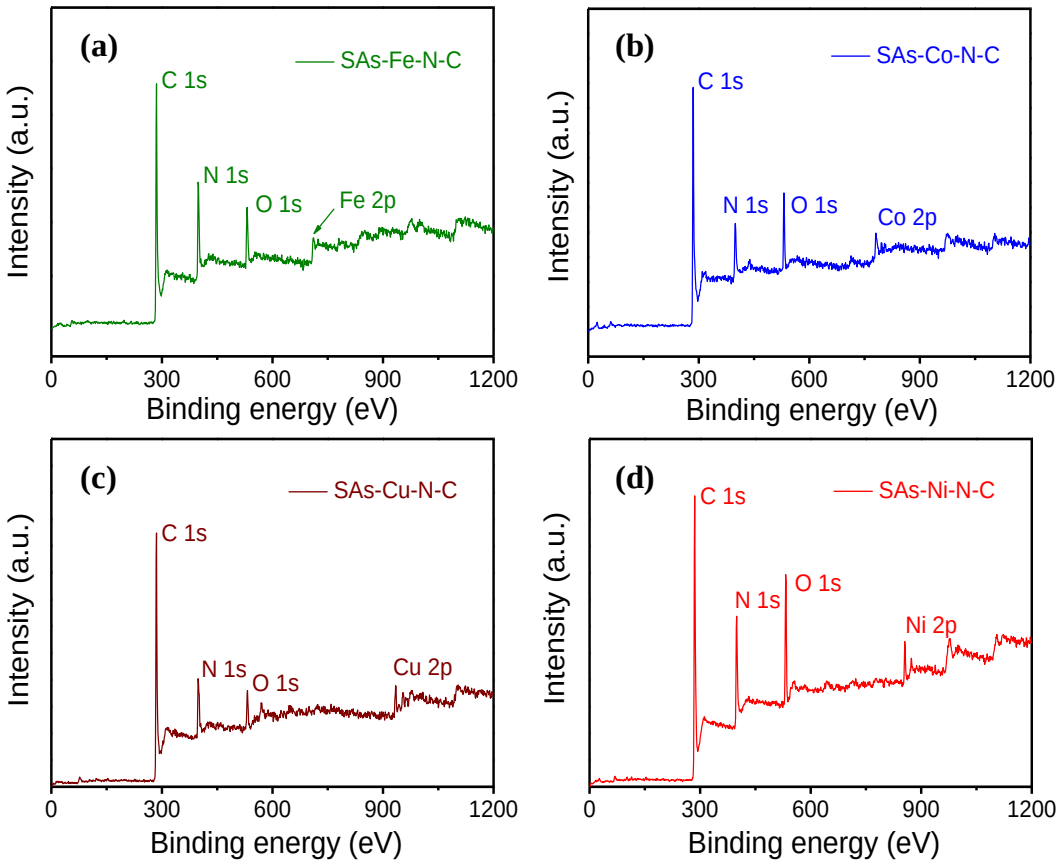

Fig. S4 XPS survey spectra of (**a**) SAs-Fe-N-C, (**b**) SAs-Co-N-C, (**c**) SAs-Cu-N-C, and (**d**) SAs-Ni-N-C

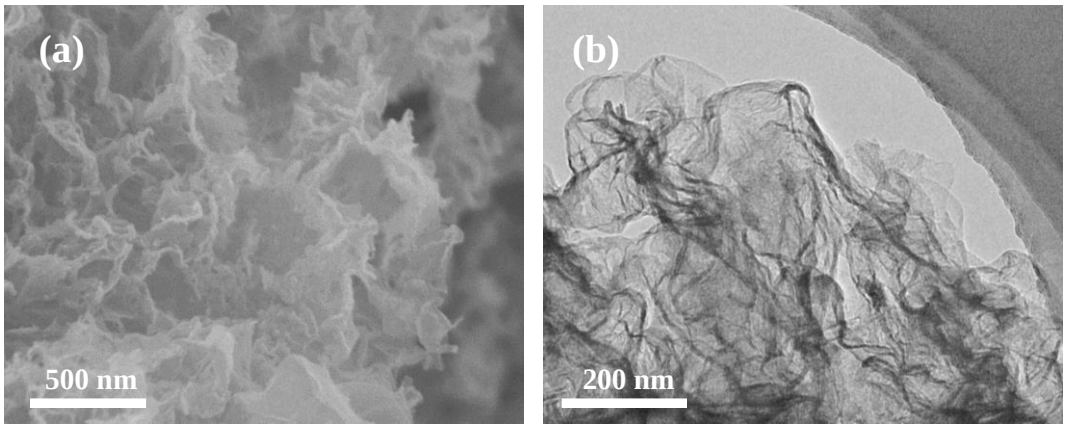

Fig. S5 (**a**) FESEM and (**b**) TEM images of N-C

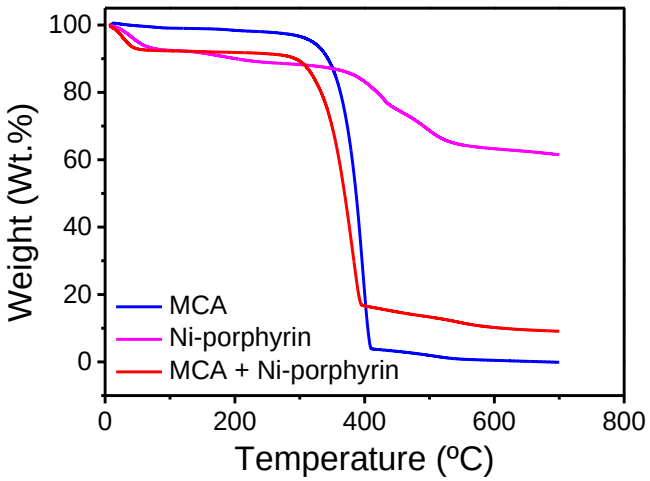

Fig. S6 TGA curves of MCA, Ni-porphyrin, and composite of MCA and Ni-porphyrin

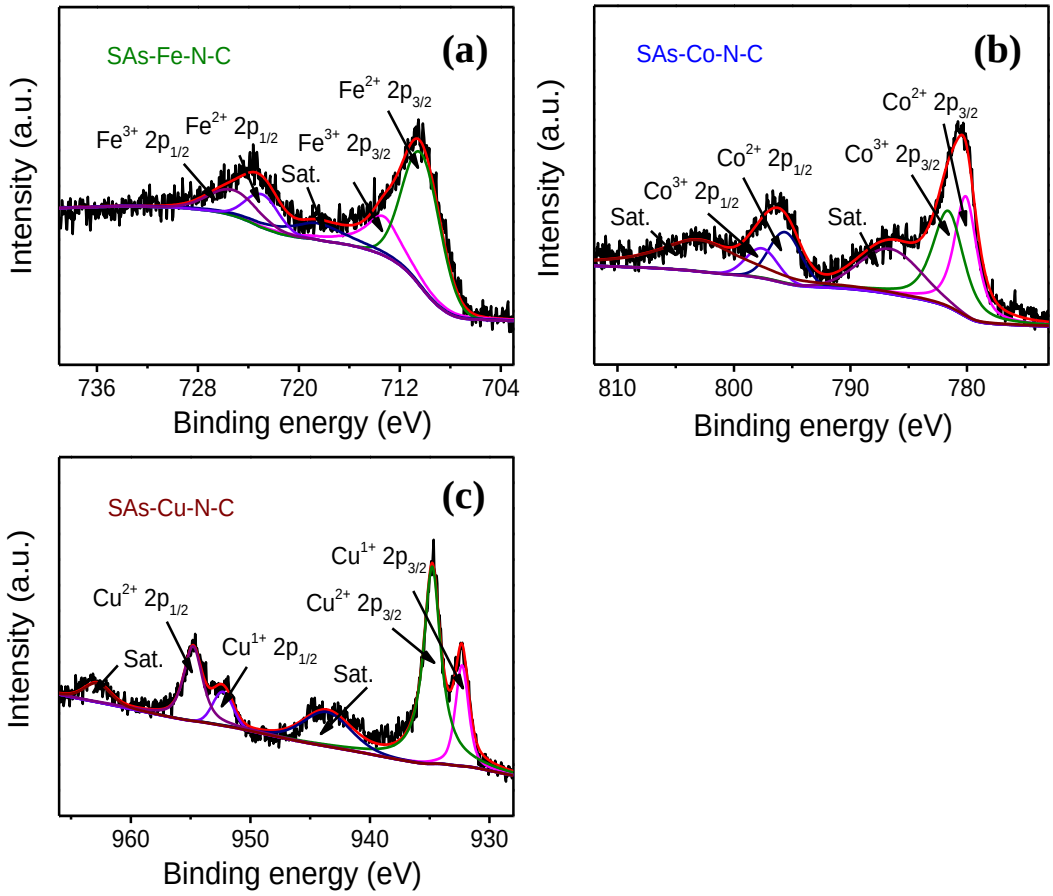

Fig. S7 High resolution metal XPS spectra of (**a**) SAs-Fe-N-C, (**b**) SAs-Co-N-C, and (**c**) SAs-Cu-N-C

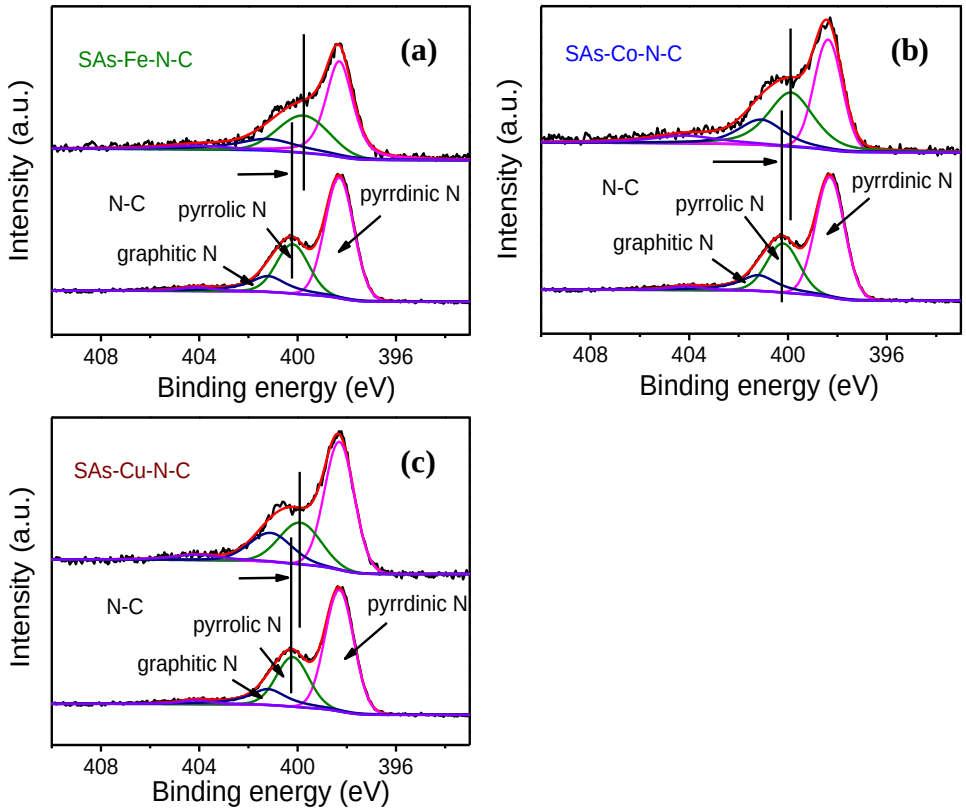

Fig. S8 High resolution N 1s XPS spectra of (**a**) SAs-Fe-N-C, (**b**) SAs-Co-N-C, and (**c**) SAs-Cu-N-C

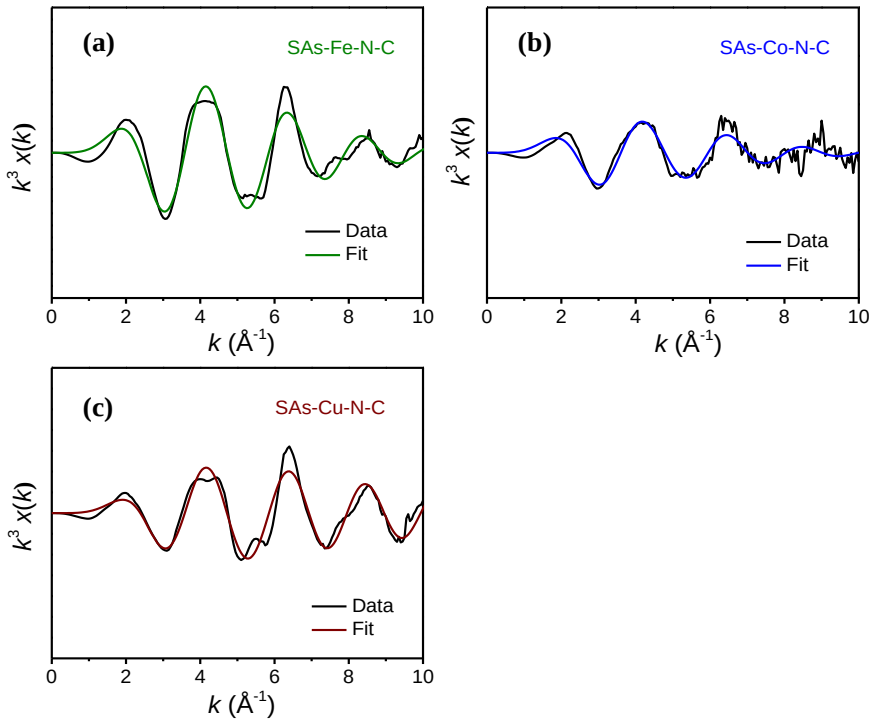

Fig. S9 FT-EXAFS fitting results of (**a**) SAs-Fe-N-C, (**b**) SAs-Co-N-C, and (**c**) SAs-Cu-N-C

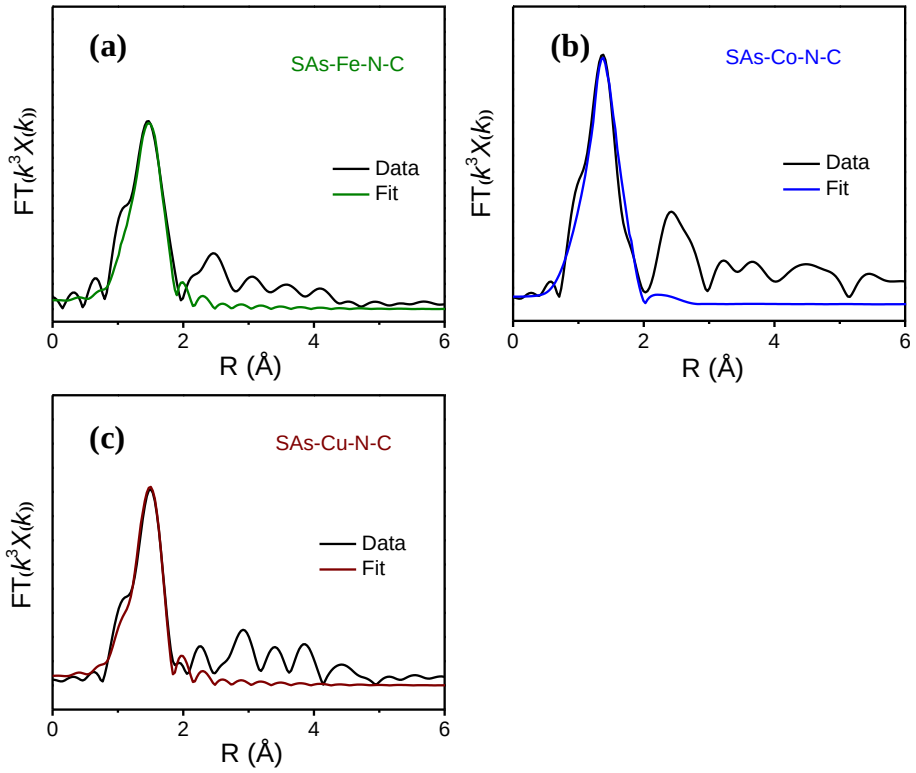

Fig. S10 FT-EXAFS fitting results of (**a**) SAs-Fe-N-C, (**b**) SAs-Co-N-C, and (**c**) SAs-Cu-N-C

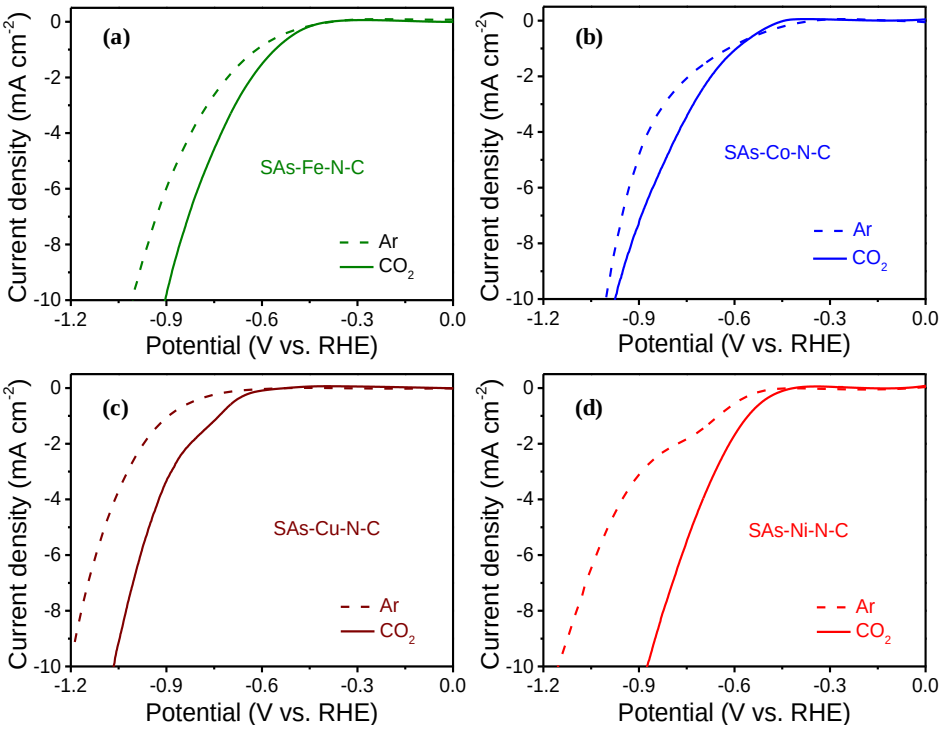

Fig. S11 LSV curves measured in CO_2 and Ar saturated 0.5 M $KHCO_3$ solutions of (**a**) SAs-Fe-N-C, (**b**) SAs-Co-N-C, (**c**) SAs-Cu-N-C, and (**d**) SAs-Ni-N-C

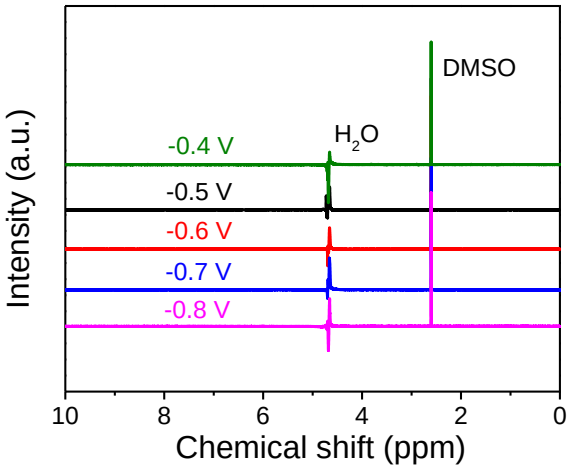

Fig. S12 ^{1}H NMR results of SAs-Ni-N-C catalyzed CO_2ER.

The total F.E. of gaseous CO and H_2 products in SAs-Ni-N-C catalyzed CO_2ER was calculated to be 100%. Likewise, the gaseous CO and H_2 products with 100% F.E. were observed for the SAs-Fe-N-C, SAs-Cu-N-C, and SAs-Co-N-C catalyzed one, respectively. Taking SAs-Ni-N-C as an example, all liquid-phase products under investigated potentials were measured by ^{1}H NMR spectra, during which the 0.5 M $KHCO_3$ electrolyte after long-term CO_2ER electrolysis was mixed with internal standard of DMSO in D_2O, and then the mixture was directly identified on ^{1}H NMR. As shown in Fig. S12, the ^{1}H NMR spectra of 0.5 M $KHCO_3$ electrolyte from the SAs-Ni-N-C catalyzed CO_2ER under applied potentials only exhibited the signals of H_2O and DMSO, no characteristic peaks of any liquid-phase CO_2ER products was observed, which excluded the formation of liquid-phase products in the SAs-Ni-N-C catalyzed CO_2ER electrolysis.

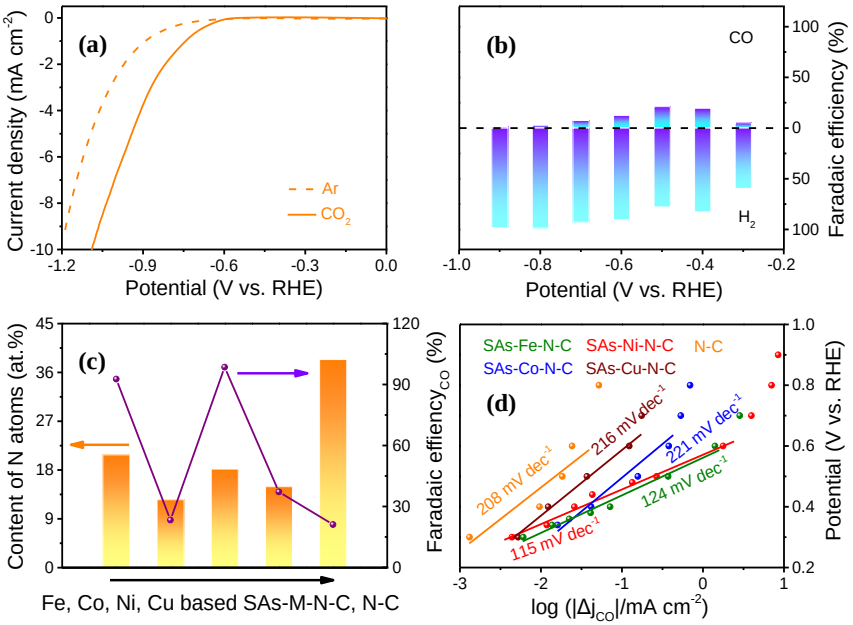

Fig. S13 LSV curves measured in CO_2 and Ar saturated 0.5 M $KHCO_3$ solutions for (**a**) N-C, (**b**) F.E. of CO and H_2 products of N-C, (**c**) content of N dopants and

maximum CO F.E. and (**d**) Tafel slopes of SAs-Fe-N-C, SAs-Co-N-C, SAs-Ni-N-C, SAs-Cu-N-C, and N-C

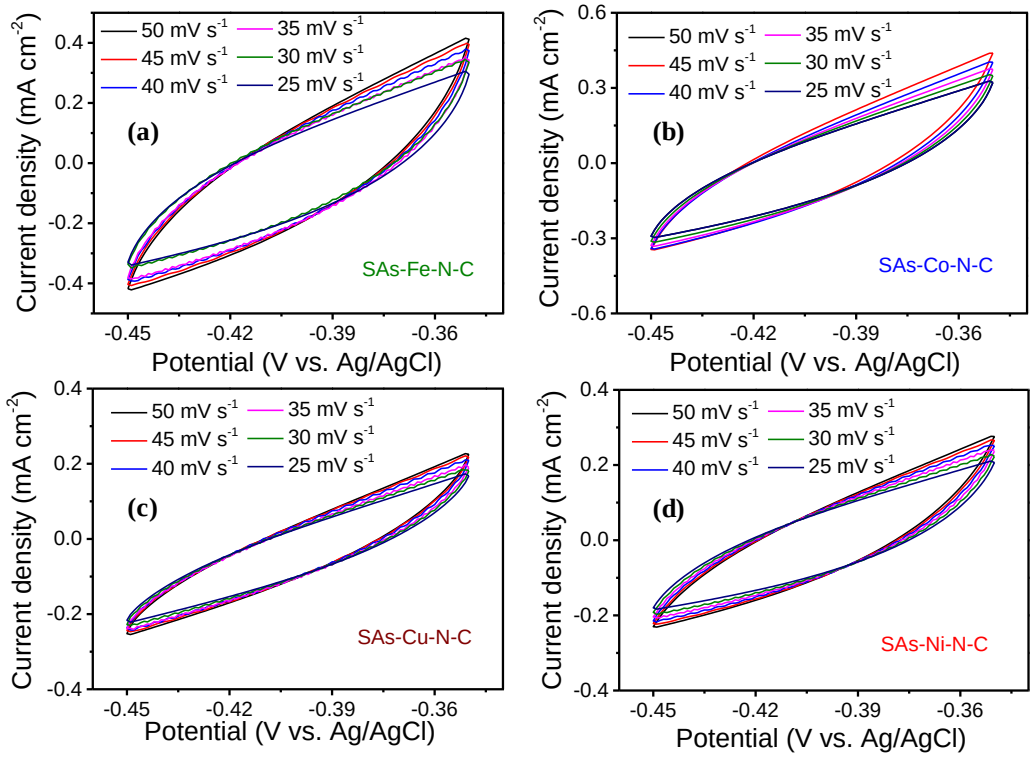

Fig. S14 CV curves measured with different scan rates at the potential of -0.35 V ~ -0.45 V vs. Ag/AgCl of (**a**) SAs-Fe-N-C, (**b**) SAs-Co-N-C, (**c**) SAs-Cu-N-C, and (**d**) SAs-Ni-N-C

The ECSA was calculated by the following equation [S1]:

$$ECSA = R_f \cdot S$$

The R_f (roughness factor) is calculated by $R_f = C_{dl}/C_s$, where C_s is the specific capacitance (21 μF cm^{-2}) of graphene [S2], S is the geometric active area (1 × 1 cm^2). The ECSA of SAs-Fe-N-C, SAs-Co-N-C, SAs-Cu-N-C, and SAs-Ni-N-C were calculated to be 102, 98, 32, and 35 cm^2, respectively.

Table S1 Contents of center metal species in the SAs-M-N-C quantified by ICP-AES measurements

Samples	Weight (W: g)	metered volume (V_0: mL)	Concentration (C: mg L^{-1})	Dilution factor (I)	Content of metal (wt%)
SAs-Fe-N-C	0.0079	10	2.17	20	5.49
SAs-Co-N-C	0.0217	10	1.60	50	3.69
SAs-Ni-N-C	0.0514	10	1.94	100	3.77
SAs-Cu-N-C	0.0208	10	2.10	50	5.05

*Calculation of the metal amount in the SAs-M-N-C:

Taking SAs-Ni-N-C as an example, the content of metal quantified by ICP-AES was calculated with the following formula:

$$Ni\ (wt\%) = \frac{C \times V_0 \times 10^{-6}}{W} \times I \times 100\% = \frac{1.94 \times 10 \times 10^{-6}}{0.0514} \times 100 \times 100\% = 3.77\ wt\%$$

Table S2 Structural parameters of SAs-Ni-N-C, SAs-Fe-N-C, SAs-Co-N-C, and SAs-Cu-N-C extracted from the EXAFS fitting results. (S_0^2 = 0.85)

Sample	Scattering pair	CN	R(Å)	σ^2 (10^{-3}Å^2)	ΔE_0 (eV)	R factor
SAs-Ni-N-C	Ni-N	4.1±0.6	2.10±0.02	4.6±0.9	-3.5±1.1	0.01
SAs-Fe-N-C	Fe-N	4.1±0.6	1.91±0.02	4.7±0.9	-3.5±1.1	
SAs-Co-N-C	Co-N	3.8±0.9	1.90±0.02	6.4±1.0	-5.7±1.1	
SAs-Cu-N-C	Cu-N	4.1±0.7	1.92±0.02	5.6±0.6	-4.1±0.8	

S_0^2 is the amplitude reduction factor; CN is the coordination number; R is interatomic distance (the bond length between central atoms and surrounding coordination atoms); σ^2 is Debye-Waller factor (a measure of thermal and static disorder in absorber-scatterer distances); ΔE_0 is edge-energy shift (the difference between the zero kinetic energy value of the sample and that of the theoretical model). R factor is used to value the goodness of the fitting.

Table S3 Comparison of CO_2ER performance and stability of SAs-Ni-N-C with other reported M-N-C catalysts for CO production

Catalyst	Onset potential (V vs. RHE)	F.E. (%)	Tafel slope (mV dec^{-1})	Stability (h)	Ref.
SAs-Ni-N-C	-0.3	98.5	115	50	This work
Fe^{3+}-N-C	-0.2	95.0	117	12	[S3]
Ni-N_4-C	-0.4	99.0	103	30	[S4]
NiN-GS	-0.35	93.2	139	20	[S5]
Ni SAs/N-C	-0.57	71.9	249	60	[S6]
Ni-NG	-0.31	95.0	110	20	[S7]
Ni^{2+}@NG	-0.38	92.0	142	20	[S8]
Ni-NCB	-0.4	99.0	101	24	[S9]
Co-TPP	-0.46	83.0	255	4	[S10]
Cu–N_2/GN	-0.33	81.0	245	10	[S11]

Supplementary References

[S1] S. Gao, Y. Lin, X. Jiao, Y. Sun, Q. Luo et al., Partially oxidized atomic cobalt layers for carbon dioxide electroreduction to liquid fuel. Nature **529**(7584), 68-71 (2016). https://doi.org/10.1038/nature16455

[S2] H.B. Yang, S.F. Hung, S. Liu, K. Yuan, S. Miao et al., Atomically dispersed Ni (I) as the active site for electrochemical CO_2 reduction. Nat. Energy **3**(2), 140-147 (2018). https://doi.org/10.1038/s41560-017-0078-8

[S3] J. Gu, C.S. Hsu, L. Bai, H. Chen, X. Hu, Atomically dispersed Fe^{3+} sites catalyze efficient CO_2 electroreduction to CO. Science **364**(6445), 1091 (2019). https://doi.org/10.1126/science.aaw7515

[S4] X. Li, W. Bi, M. Chen, Y. Sun, H. Ju et al., Exclusive ni-n4 sites realize near-unity CO selectivity for electrochemical CO_2 reduction. J. Am. Chem. Soc. **139**(42), 14889-14892 (2017). https://doi.org/10.1021/jacs.7b09074

[S5] K. Jiang, S. Siahrostami, A.J. Akey, Y. Li, Z. Lu et al., Transition-metal single atoms in a graphene shell as active centers for highly efficient artificial photosynthesis. Chem **3**(6), 950-960 (2017).

https://doi.org/10.1016/j.chempr.2017.09.014

[S6] C. Zhao, X. Dai, T. Yao, W. Chen, X. Wang et al., Ionic exchange of metal-organic frameworks to access single nickel sites for efficient electroreduction of CO_2. J. Am. Chem. Soc. **139**(24), 8078-8081 (2017). https://doi.org/10.1021/jacs.7b02736

[S7] K. Jiang, S. Siahrostami, T. Zheng, Y. Hu, S. Hwang et al., Isolated Ni single atoms in graphene nanosheets for high-performance CO_2 reduction. Energy Environ. Science **11**(4), 893-903 (2018). https://doi.org/10.1039/c7ee03245e

[S8] W. Bi, X. Li, R. You, M. Chen, R. Yuan et al., Surface immobilization of transition metal ions on nitrogen-doped graphene realizing high-efficient and selective CO_2 reduction. Adv. Mater. **30**(18), e1706617 (2018). https://doi.org/10.1002/adma.201706617

[S9] T. Zheng, K. Jiang, N. Ta, Y. Hu, J. Zeng, J. Liu, H. Wang, Large-scale and highly selective CO_2 electrocatalytic reduction on nickel single-atom catalyst. Joule. **3**(1), 265-278 (2019). https://doi.org/10.1016/j.joule.2018.10.015

[S10] X Hu, M. Ronne, S.U. Pedersen, T. Skrydstrup, K. Daasbjerg. Enhanced catalytic activity of cobalt porphyrin in CO_2 electroreduction upon immobilization on carbon materials. Angew. Chem. Int. Ed. **56**(23), 6468-6472 (2017). https://doi.org/10.1002/anie.201701104

[S11] W. Zheng, J. Yang, H. Chen, Y. Hou, Q. Wang et al., Atomically defined undercoordinated active sites for highly efficient CO_2 electroreduction. Adv. Funct. Mater. **30**(4), 1907658 (2019). https://doi.org/10.1002/adfm.201907658